Structures of a Semidilute Polymer Solution under Oscillatory Shear Flow

Shin Saito, Katsuo Matsuzaka,† and Takeji Hashimoto*

Department of Polymer Chemistry, Graduate School of Engineering, Kyoto University, Kyoto 606-8501, Japan

Received January 12, 1999; Revised Manuscript Received April 30, 1999

ABSTRACT: The structures of a semidilute polymer solution, comprised of ultrahigh molecular weight polystyrene as a solute and dioctyl phthalate as a solvent, under oscillatory shear flow were investigated by means of small-angle light scattering. The system exhibited a double-winged anisotropic scattering pattern called "butterfly", characteristic of shear-induced phase separation known to occur under a continuous shear flow. Under oscillatory shear flow the phase separation strongly depended on both a strain amplitude γ_0 and an angular frequency ω, being observed inside a quasi-parabolic line in the space of γ_0 vs log ω. The system was brought to a *dynamically* stationary state in about 20 min after applying the shear flow, and the shear-induced structures changed with a strain phase ϕ of the oscillatory shear. At a given ϕ and γ_0, the shear-induced structures strongly depended on ω: the characteristic wavelength of the structures decreased with increasing ω, and the mean square of the concentration fluctuations was a maximum at a certain ω.

I. Introduction

It is well-known that entangled polymer solutions in a single phase exhibit enhancement of concentration fluctuations or phase separation when shear flow is imposed. This is called shear-induced concentration fluctuations and/or phase separation, and recently a great deal of attention has been focused on this intriguing nonequilibrium phenomenon to gain insight into the underlying physics.

In experimental studies, Hashimoto et al. studied by small-angle light scattering the time evolution of shear-induced structures after imposing shear flow and the shear-rate-dependent structures after the achievement of steady state.[1−4] A periodic structure developed by shear flow was visualized in situ under optical microscopy. Two-dimensional Fourier transform of the micrograph proved that the observed structure is the origin of a "butterfly pattern", which is the unique scattering pattern typical of shear-induced phase separation.[5]

In theoretical studies, Helfand and Fredrickson argued that this phenomenon is a shear-enhanced concentration fluctuations as a consequence of the coupling between the stress field and the polymer concentration field.[6] Onuki introduced a tensor variable to represent chain deformation and suggested a dynamic model and applied it to this phenomenon.[7−10]

Despite these experimental and theoretical efforts, we are still far from a complete understanding of the mechanism of this phenomenon. A key to understanding this phenomenon is as follows. In a quiescent semidilute polymer solution, there are thermal concentration fluctuations, as indicated in Figure 1, giving rise to regions of higher and lower polymer concentrations which have a higher and lower concentration of entanglement points, respectively. When shear flow is imposed on such a system, the stress tends to become higher in the more entangled regions because of the coupling between concentration fluctuations and stress. The stress or the elastic free energy stored by deformation of the entangled polymer chains is relaxed by disentanglement when the shear rate $\dot{\gamma}$ is lower than the terminal relaxation rate τ_m^{-1}. However, if $\dot{\gamma}$ is higher than τ_m^{-1}, the elastic free energy is released only by the solvent squeezing from the more entangled regions.[7−10] The higher the concentration, the larger the stored elastic free energy and hence the more is the solvent squeezing. As a result, the concentration fluctuations are built up under shear, if $\dot{\gamma}$ is larger than a critical shear rate $\dot{\gamma}_c$ of the system ($\dot{\gamma}_c \cong \tau_m^{-1}$). If $\dot{\gamma}$ is increased above $\dot{\gamma}_c$, a shear-induced phase separation is eventually brought about.

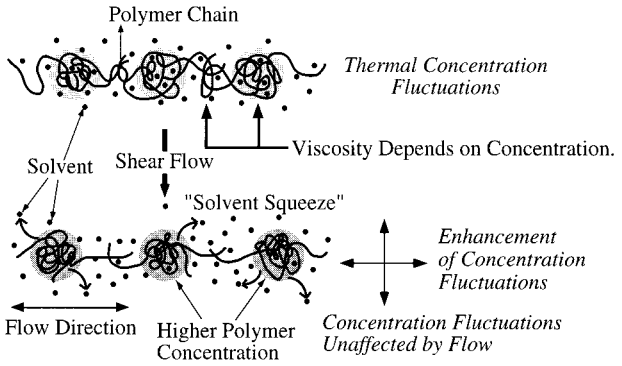

Figure 1. Schematic representation of the origin of shear-induced phase separation.

So far, most of the experimental studies have been carried out by means of small-angle light scattering,[1−4,11−17] optical microscopy,[5,14] and rheology measurements[4,18,19] at a constant shear rate (continuous shear flow), and only a few attempts have been made to apply other kinds of shear field, e.g., an oscillatory shear flow. These kinds of shear flow are different in that the strain γ of the continuous shear flow increases in proportion to time with $\dot{\gamma}$ constant, while γ and $\dot{\gamma}$ of the oscillatory shear flow change sinusoidally with a 90°

* To whom correspondence should be addressed.
† Present address: Sekisui Chemical Co., Ltd., 2-2, Kamichoshi-cho, Kamitoba, Minami-ku, Kyoto 601-8105, Japan.

10.1021/ma990031i CCC: $18.00
Published on Web 07/02/1999

phase shift. We shall point out below essential differences between the continuous and oscillatory shear flow concerning structural changes by shear flow.

Suppose that a Fourier mode of concentration fluctuations having wavelength Λ has the relaxation rate $\tau^{-1}(\Lambda)$. When a continuous shear flow of shear rate $\dot{\gamma}$ is imposed on a system, all the Fourier modes of the concentration fluctuations having $\tau^{-1}(\Lambda) < \dot{\gamma}$ are affected by the shear flow. On the other hand, when an oscillatory shear flow of angular frequency ω is imposed on a system, only the modes of concentration fluctuation having $\tau^{-1}(\Lambda) \sim \omega$ would be dominantly affected by the shear flow. This is because the modes of the concentration fluctuations having $\tau^{-1}(\Lambda) \gg \omega$ decay before they are deformed by the shear flow, and hence they are unaffected by shear, while the modes of the concentration fluctuations having $\tau^{-1}(\Lambda) \ll \omega$ cannot respond to the applied deformation since the concentration fluctuations cannot be enhanced as a result of a solvent squeezing mechanism as will be detailed later. Thus, an oscillatory shear flow picks up a response of particular modes of the concentration fluctuations, while a continuous shear flow does not.

In addition, an oscillatory shear experiment provides more information than a continuous shear experiment. For example, an oscillatory shear experiment (dynamic viscoelastisity) gives us a storage modulus G' and a loss modulus G'', while a continuous shear experiment gives us only a shear modulus. Angular frequency dependencies of G' and G'' provide us a relaxation spectrum, a most important rheological property. Therefore, we might get further information on the static and dynamic properties of shear-induced structures using an oscillatory shear flow if we can measure the phase lag between the strain and the stress or between the strain and the scattering.

For reasons mentioned above, we believe that the study under oscillatory shear flow plays an important role in understanding of physics of shear-induced concentration fluctuations and/or phase separation. We employed a semidilute solution of polystyrene prepared with dioctyl phthalate (DOP) as a solvent. The solution has the same characteristics as that used in the continuous shear flow experiments.[3,4,11] We report here the results obtained with small-angle light scattering experiments. Combined rheological and structural analyses will be taken up in companion papers.

Whether the phenomena to be discussed are attributed to the shear-induced phase separation or the shear-induced concentration fluctuations in a single phase is immaterial in this paper. However, the phenomena can be regarded as a phase separation at least for some cases, judging from the following results.

First, we have performed experiments under oscillatory shear flow using small-angle neutron scattering (SANS), which enables us to observe Fourier modes of the fluctuations in the q region larger than 0.02 nm^{-1}. We have found that a butterfly pattern could be obtained even in the SANS q region under high-angular frequency oscillatory shear. We have found that the scattering profiles parallel to the flow direction were described by a linear combination of a Ornstein−Zernike function, which expresses scattering from concentration fluctuations in a single phase, and a squared Lorentzian function, which gives scattering from random two-phase structures. This result signifies that the shear-induced structures have an interface between two phases rich and poor in polymer concentration with a finite interface thickness.[21]

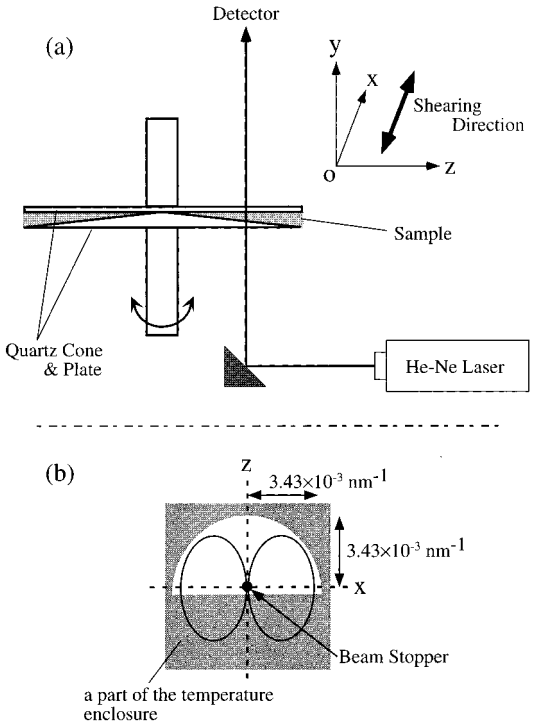

Figure 2. (a) Schematic diagram of the experimental setup. The *ox* axis is parallel to the shearing direction, the *oy* axis to shear gradient direction, and the *oz* axis to the vorticity or neutral direction. The incident beam was sent along the *oy* axis, and the two-dimensional scattering pattern is detected by a CCD camera with its detector plane set parallel to the *oxz* plane. (b) Due to the optical setup, the q range for the scattered beam is limited inside the half-circle with a radius of $q = 3.43 \times 10^{-3}$ nm^{-1}.

Second, we have already reported small-angle light scattering studies of the time evolution of shear-induced structures after onset of a continuous shear flow of a constant shear rate.[4] After some incubation period, a scattering peak appeared, the magnitude of the scattering vector at the scattering peak decreased with time, and the peak intensity increased with time. These values finally reached the steady-state values. These behaviors are very similar to the system undergoing a phase separation via spinodal decomposition for a thermodynamically unstable solution without shear.

II. Experimental Method

A. Sample. Ultrahigh molecular weight polystyrene (PS), coded PS548, used in the present study had a weight-average molecular weight M_w of 5.48×10^6 and a heterogeneity index $M_w/M_n = 1.15$, where M_n is the number-average molecular weight. A solution containing 6.0 wt % of PS548 was prepared using DOP as a solvent, which is a Θ solvent for PS at 22 °C. The concentration is about 40 times the overlap concentration c^*.

The solution has an upper critical solution temperature (UCST) type phase diagram with a cloud point of 13.8 °C. The experiments were carried out at 27 °C, at which the solution is in a single phase in quiescence.

B. Shear Light Scattering. Figure 2a shows a schematic diagram of the shear small-angle light scattering apparatus used in this experiment where the flow is imposed along $\pm ox$ axis and the velocity gradient exists parallel to *oy* axis. Details of this apparatus was reported elsewhere.[20] It consists of a cone and plate made of quartz with radii of 40 mm and a cone angle of 1.0°. The cone and plate containing the sample are covered

by a temperature-controlled enclosure. A He−Ne laser with a wavelength of 632.8 nm is used as an incident beam source. The incident beam is sent along the velocity gradient direction (*oy* axis). The scattered light is captured by a cooled charge coupled device (CCD) camera as a two-dimensional detector, the detecting plane of which is set parallel to the *oxz* plane.

Due to the optical setup of this apparatus, the wavenumber range or q range is limited, where q is defined by $q \equiv (4\pi/\lambda)\sin(\theta/2)$ with λ and θ being the wavelength of light and the scattering angle in medium. As shown in Figure 2b, the q range we can observe exists inside the half circle with the radius of $q = 3.43 \times 10^{-3}$ nm^{-1}.

Scattering experiments were performed as follows. Oscillatory shear flow of a fixed strain amplitude γ_0 and an angular frequency ω was imposed on the system. The strain γ and the shear rate $\dot{\gamma}$ are given by the following equations as a function of ω and time t.

$$\gamma(t) = \gamma_0 \sin \omega t = \gamma_0 \sin \phi \tag{1}$$

$$\dot{\gamma}(t) = \gamma_0 \omega \cos \omega t = \gamma_0 \omega \cos \phi \tag{2}$$

where ϕ is the strain phase angle. If the shear flow expressed by eqs 1 and 2 was imposed on the solution, the oscillating shear stress $\sigma(t)$ and the scattering intensity $I(\mathbf{q};t)$ were developed. Here, $\mathbf{q}$ denotes a scattering wave vector whose amplitude is defined earlier. Taking into account nonlinearity, $\sigma(t)$ and $I(\mathbf{q};t)$ are generally expressed by Fourier series

$$\sigma(t) = \sum_{i=1}^{\infty} \sigma_i \sin[\omega_i t + \delta_{\sigma,i}(t)] \tag{3}$$

$$I(\mathbf{q};t) = I_s(\mathbf{q}) + \sum_{i=1}^{\infty} \Delta I_i(\mathbf{q};t) \sin[\omega_i t + \delta_{I,i}(t)] \tag{4}$$

where σ_i, ω_i, $\delta_{\sigma,i}$, $\delta_{I,i}$, and $\Delta I_i(\mathbf{q};t)$ are the stress, angular frequency, phase difference between the strain and the stress, phase difference between the strain and the scattering intensity, and excess scattering from the quiescent state for the ith Fourier mode, respectively, and $I_s(\mathbf{q})$ is the static scattering intensity at the quiescent state at $\mathbf{q}$. In about 20 min after applying the shear flow, the dynamic response of the scattering intensity becomes stationary with t, which we call a *dynamic* steady state. We measured the scattering patterns and their intensity distributions at the dynamic steady state as a function of γ_0 and ω and determined whether the shear flow induces a phase separation. In the case when the shear-induced butterfly pattern was observed, the scattered intensity distribution was measured at a particular strain phase interval between $\phi - \Delta\phi$ and $\phi + \Delta\phi$ at the dynamic steady state. Thus, we limit our discussion to the dynamic steady-state structures induced by the oscillatory shear flow in this paper. Time evolution of the structures after onset of an oscillatory shear flow will be reported elsewhere.

C. Rheological Properties. We measured the linear dynamic rheological properties and the steady-state viscosity η of the system at the same temperature (27 °C) as that at which the light scattering experiments were carried out. The strain amplitude γ_0 used here was 0.2, which is within the limits of linear viscoelasticity. Figure 3 shows the absolute amplitude of complex dynamic shear viscosity $|\eta^*|$, the storage modulus G', and the loss modulus G'' of the solution as a function of ω and η as a function of $\dot{\gamma}$. The expected scaling laws in the terminal regime $G' \sim \omega^2$ and $G'' \sim \omega^1$ were not observed at the low-ω limit covered for this polymer solution.

It may be worth pointing out how to estimate the longest relaxation time τ_m from these data. One can find in $|\eta^*|$ that there is a ω ($\cong$0.1 rad/s) at which the slope of the ω dependence of $|\eta^*|$ changes. This ω also satisfies $\tan\delta \cong 1$. We suppose that τ_m could be obtained by $\tau_m = 1/\omega \cong 10$ s. We also suppose that the ω region below 0.1 rad/s, where the Newtonian behavior should be naturally expected, reflects the response

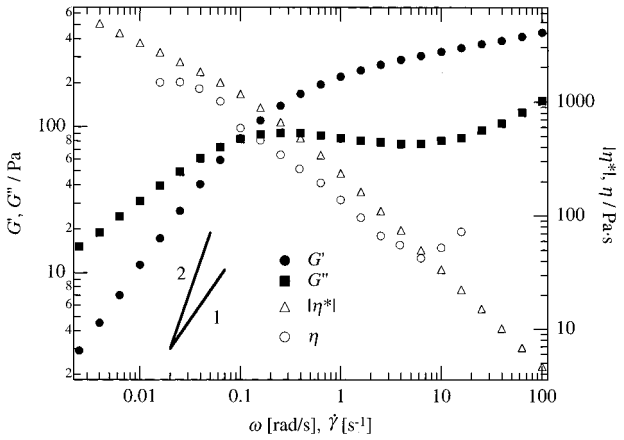

Figure 3. Linear viscoelastic properties, G', G'', $|\eta^*|$, and the steady-state viscosity η of PS548/DOP 6.0 wt % at 27 °C as a function of frequency ω or shear rate $\dot{\gamma}$.

from the large-scale concentration fluctuations, and hence the upturn toward the low-ω limit was observed. Furthermore, the non-Newtonian behavior in η was observed above about $\dot{\gamma} = 0.04$ s^{-1}, which is not far from $\omega = 0.1$ rad/s when the viscosities obtained by the steady shear experiment and the dynamic shear experiment are compared on the basis of the Cox−Mertz rule. This might indicate the validity of the estimation of τ_m from $|\eta^*|$. Therefore, we use 10 s as τ_m in this paper.

III. Results

A. Shear-Induced Phase Separation as a Function of Strain Amplitude and Angular Frequency. First, we have to explore under what conditions the oscillatory shear flow induces phase separation. Therefore, we investigated whether shear-induced phase separation occurs as a function of γ_0 and ω.

Figure 4 shows an example of the observed scattering patterns at a representative strain phase $\phi = 90°$, i.e., at the maximum shear strain. The left and right columns represent the γ_0 dependence of the scattering pattern for a given $\omega = 0.6309$ rad/s and ω dependence of the scattering pattern for a given $\gamma_0 = 2.2$, respectively. The scattering intensities for $\gamma_0 = 0.2$ (Figure 4a) and $\gamma_0 = 1.2$ (Figure 4b) at $\omega = 0.6309$ rad/s were almost the same as that in quiescence, while an anisotropic scattering pattern called the "butterfly pattern" was observed for $\gamma_0 = 2.2$ (Figure 4c). This butterfly pattern is characteristic of shear-induced phase separation. The right column indicates that a butterfly pattern was observed at $\omega = 0.6309$ rad/s (Figures 4e), while not at a lower $\omega = 0.06309$ rad/s (Figures 4d) or at a higher $\omega = 15.85$ rad/s (Figure 4f). This indicates that at the fixed γ_0 and ϕ the shear-induced phase separation does not occur at too high or too low ω.

An appearance of a butterfly pattern is summarized in Figure 5 with γ_0 as a vertical axis and log ω as a horizontal axis. The observation of the butterfly patterns was performed at $\phi = 0°$ and 90°. The open circles show that a butterfly pattern was observed, the open triangles that a weak scattering was obtained at higher q along the flow direction, and the crosses that the butterfly pattern did not appear. Figure 5 clearly shows that this γ_0−log ω plane is divided into two regions by a quasi-parabolic line, i.e., one-phase and two-phase regions, which is referred to as a "dynamic" phase diagram. The dynamic phase diagram reveals that the oscillatory-shear-induced phase separation occurs when γ_0 is larger

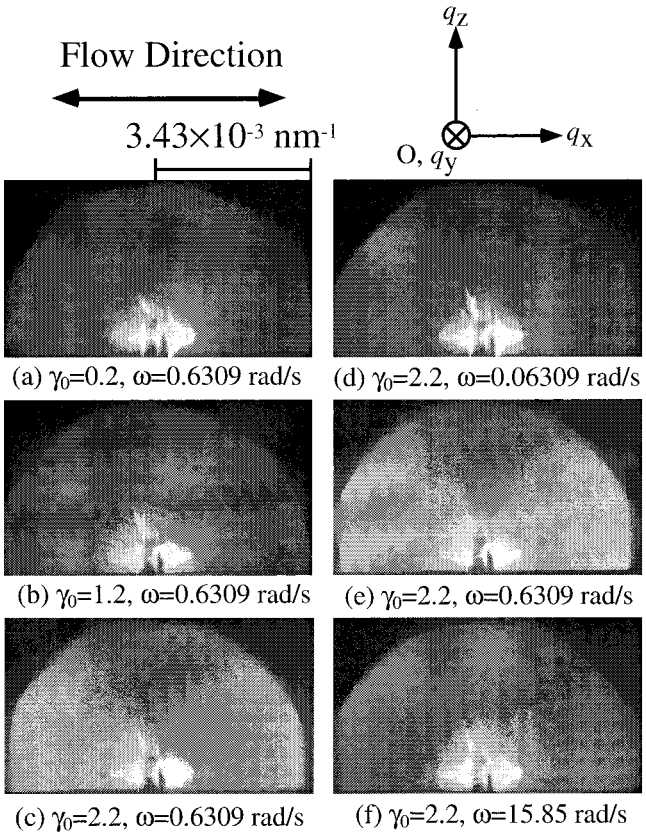

Figure 4. Scattering patterns at strain phase $\phi = 90°$ under various oscillatory conditions: in the left column (a, b, and c) γ_0 was changed at a fixed ω, and in the right column (d, e, and f) ω was changed at a fixed γ_0.

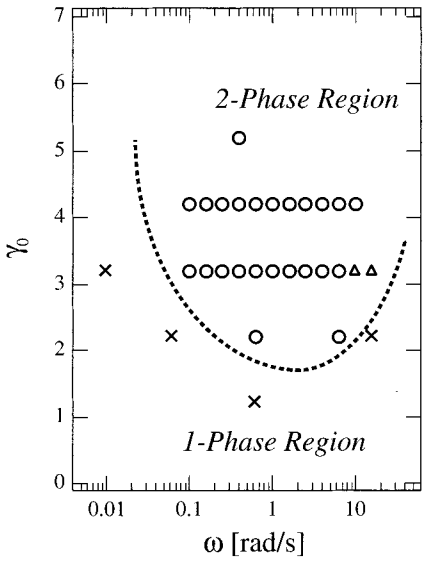

Figure 5. Summary of butterfly appearance: open circles denote a butterfly pattern could be observed, open triangles denote weak scattering was obtained at higher wavenumber along the flow direction, and crosses denote a butterfly pattern did not appear. The observation of the butterfly patterns was performed at $\phi = 0°$ and 90°. Note that the dashed line is arbitrary.

than a critical value (γ_{0c}) at a given ω and when ω is between lower and upper critical values at a given $\gamma_0 > \gamma_{0c}$.

B. Dynamics of Shear-Induced Structures in a Period of the Shearing Cycle. As γ and $\dot{\gamma}$ of the oscillatory shear flow change sinusoidally, it can be expected that the shear-induced structures also change. Here, we are concerned with the dynamic change of the butterfly pattern with the strain phase ϕ.

Figure 6 shows the ϕ dependence of scattering patterns obtained for the oscillatory shear of $\gamma_0 = 4.2$ and $\omega = 0.1$ rad/s. The butterfly pattern appeared with its maximum intensity along the flow direction at any ϕ. As ϕ increased from 0° to 90°, the butterfly pattern was clearly developed: the scattering intensity increased in the flow direction and the butterfly wings expanded, resulting in sharpening of the "dark streak"[2,3] perpendicular to flow. The dark streak means that the scattering intensity normal to flow direction was as weak as that before imposing shear, that is to say, in a single phase. As ϕ increased from 90° to 180°, on the other hand, the scattering intensity decreased and the dark streak broadened.

To investigate the ϕ dependence of the scattering intensity quantitatively, we evaluated the scattering profiles as a function of $\mathbf{q} = \mathbf{q}_{\parallel} \equiv (q_x,0,0)$ parallel to the flow direction, as shown in Figure 7. These profiles were obtained as follows: we first obtained the scattering intensity averaged around the sector (azimuthal angle of ±5°) centered around the q_x axis for the solution under the shear with $\Delta\phi = 0.57°$ ($\Delta\phi/360° = 1.58 \times 10^{-3}$), and then the sector averaged scattering intensity was obtained over the same sector angle and same time period for the solution before imposing shear; $I(q_x)$ shown in Figure 7 was obtained after subtracting the latter from the former. The top shows the profiles from $\phi = 0°$ to 90°, and the bottom shows those from 90° to 180°. All profiles have scattering peaks at $q_x = q_{mx}$, indicating that a periodic structure with a characteristic wavelength exists at each ϕ. As ϕ increased from 0° to 90°, q_{mx} moved to lower q_x and its intensity I_m increased. As ϕ increased from 90° to 180°, on the other hand, q_{mx} and I_m shifted oppositely: q_{mx} shifted to higher q_x and I_m decreased. This shows that the development and decay of the structures was synchronized with the strain phase.

We performed a similar experiment with the same $\gamma_0 = 4.2$ but another $\omega = 10$ rad/s. Figure 8 shows the ϕ dependence of the scattering pattern, indicating a similarity to that at the lower $\omega = 0.1$ rad/s; namely, the intensity of the butterfly pattern was maximum at $\phi = 90°$ and was minimum at $\phi = 0°$ and 180°. Therefore, we now see that the structures induced by the oscillatory shear flow were synchronized with the strain independently of ω covered in our experiment. However, the shape of the butterfly observed in Figure 8 was quite different from that of Figure 6. At $\phi = 0°$ an exceedingly weak butterfly was observed. With an increase of ϕ from 0° to 90°, the scattering intensity in the higher q_x region increased, but the intensity level at $\phi = 90°$ is much less than that at $\omega = 0.1$ rad/s.

Figure 9 shows the scattering profiles parallel to the flow evaluated from Figure 8, by using the same method as that mentioned above in conjunction with Figure 7 but $\Delta\phi = 28.7°$ ($\Delta\phi/360° = 8.00 \times 10^{-2}$). The figure indicates that q_{mx} at $\omega = 10$ rad/s exists at a higher q_x region than that of lower $\omega = 0.1$ rad/s and that the ϕ dependencies of q_{mx} and I_m at $\omega = 10$ rad/s were not so pronounced as those in the case of $\omega = 0.1$ rad/s shown in Figure 7. In the case of $\omega = 10$ rad/s, the response of the scattering profiles with the applied strain phase depends remarkably on q_x: in the small-q_x region $I(q_x)$ depends only weakly on ϕ, but in high-q_x region it

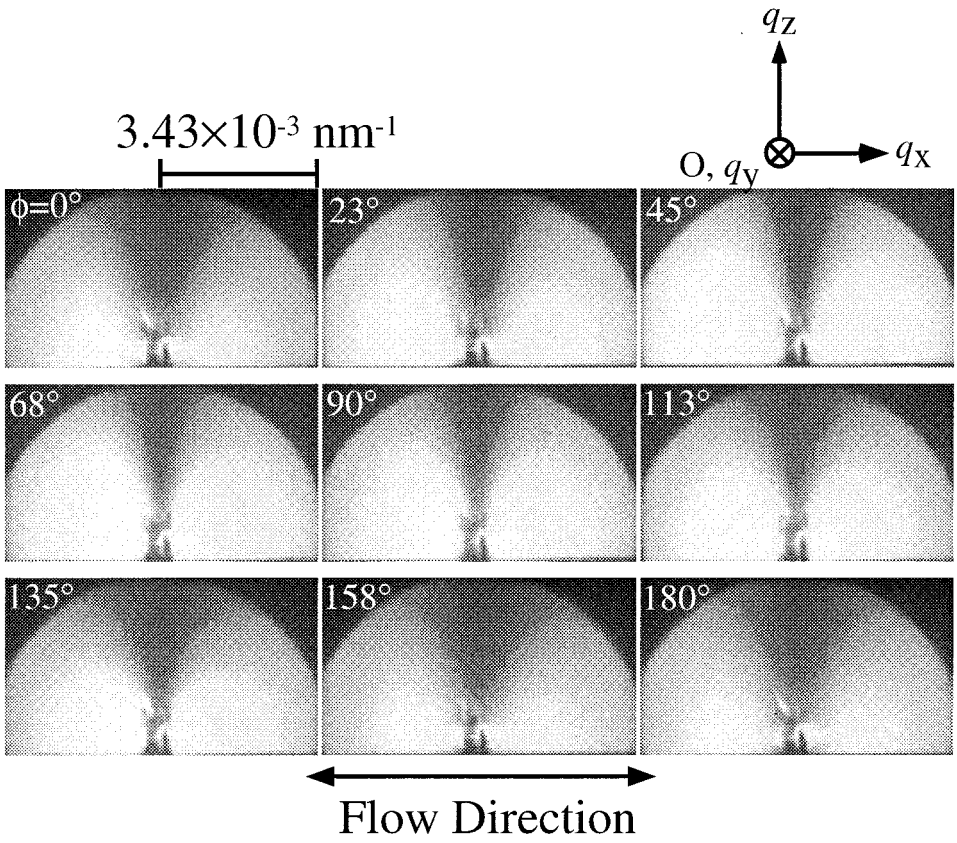

Figure 6. Scattering patterns at $\gamma_0 = 4.2$ and $\omega = 0.1$ rad/s at representative strain phases. The phase interval $\Delta\phi$ over which the patterns were taken was given by $\Delta\phi/360° = 1.58 \times 10^{-3}$.

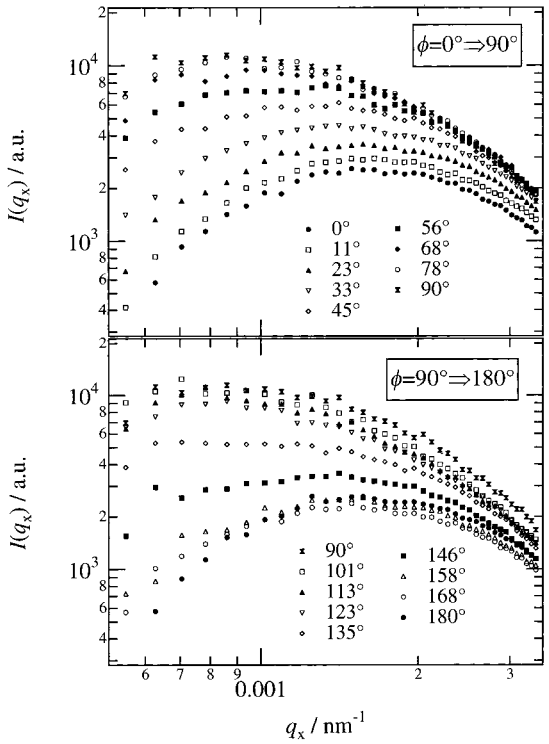

Figure 7. Scattering profiles as a function of q along the flow direction at $\gamma_0 = 4.2$ and $\omega = 0.1$ rad/s: the top represents those for ϕ from 0° to 90°, and the bottom represents those for ϕ from 90° to 180°.

depends strongly on ϕ. In the high-q_x region, the scattering intensity oscillates in harmony with ϕ, while that in the low-q_x region is nearly independent of ϕ. In other words, the large-scale structures which are reflected in the low-q_x region do not change with ϕ, while the small-scale structures which are reflected in the high-q_x region develop and decay in synchronization with strain. We also note that the scattering intensity decays with power law with a slope of nearly −2 in the low-q_x region.

Furthermore, it should be pointed out that the shape of the scattering curve around the scattering peak was sharper at $\omega = 10$ rad/s than that at $\omega = 0.1$ rad/s. This means that the size distribution of the shear-induced structures at $\omega = 10$ rad/s were narrower than that at $\omega = 0.1$ rad/s.

C. Angular Frequency Dependence of Shear-Induced Structures. Since the development and decay of the structures induced by oscillatory shear flow was synchronized with strain, we may now consider the ω dependence of the structures at a given γ_0 and ϕ.

Figure 10 shows the scattering profiles in the flow direction taken at various ω at representative ϕ: $\phi = 0°$ (the top) and $\phi = 90°$ (the bottom). γ_0 was fixed at 4.2. The arrows indicate the peak positions q_{mx} of the scattering profiles. Clearly, the shape of scattering profiles varies with ω. Here we note that q_{mx} moved to higher q_x with increasing ω, while I_m took a maximum at $\omega = 0.6309$ rad/s.

To consider this behavior quantitatively, we show I_m and the characteristic wavelength of a periodic structure $\Lambda_{mx} \equiv 2\pi/q_{mx}$ as a function of ω in Figure 11. For both ϕ, Λ_{mx} decreases with increasing ω, indicating that the structures become smaller as ω increases. On the other hand, I_m takes a maximum at $\omega = 0.6309$ rad/s. This implies that the amplitude of concentration fluctuation, i.e., the contrast between two phases, reaches a maximum at $\omega = 0.6309$ rad/s.

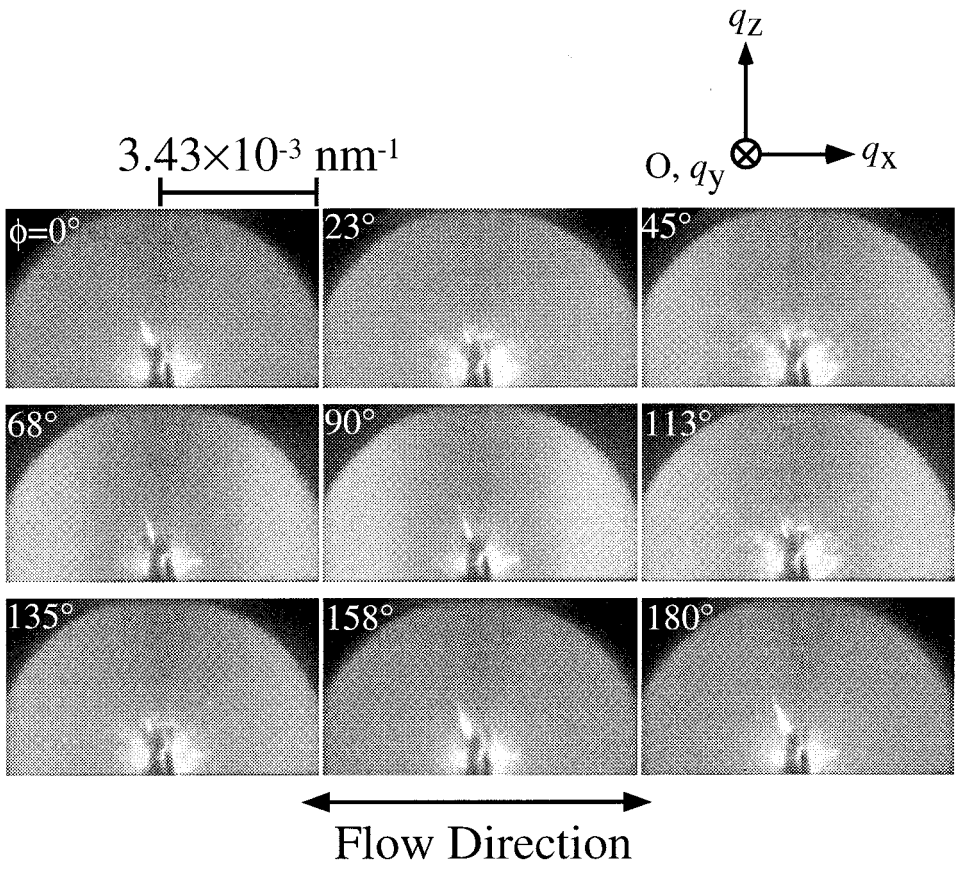

Figure 8. Scattering patterns at $\gamma_0 = 4.2$ and $\omega = 10$ rad/s at representative strain phases. $\Delta\phi/360° = 7.80 \times 10^{-2}$.

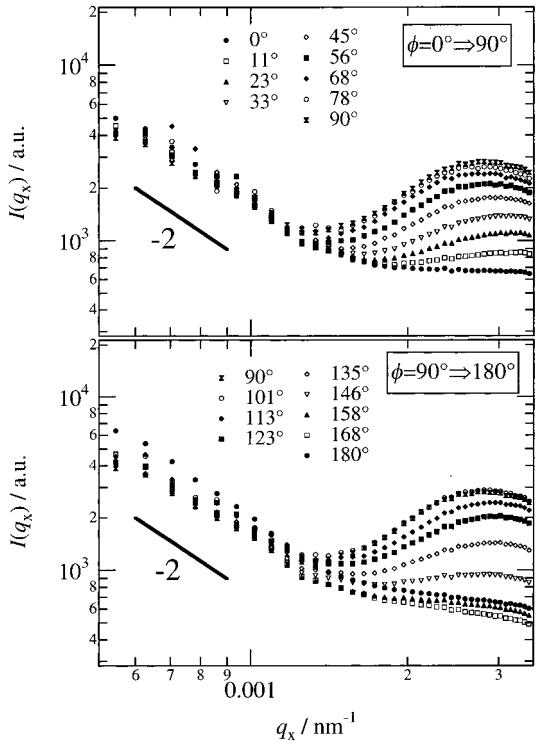

Figure 9. Scattering profiles as a function of q along the flow direction at $\gamma_0 = 4.2$ and $\omega = 10$ rad/s: the top represents those for ϕ from 0° to 90°, and the bottom represents those for ϕ from 90° to 180°.

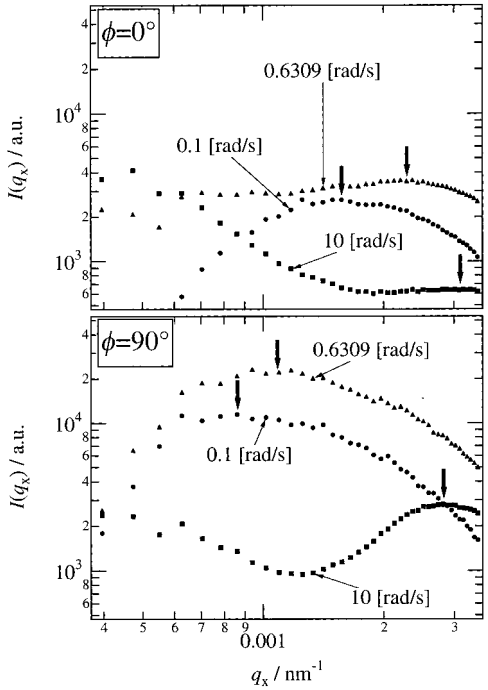

Figure 10. Frequency dependence of scattering profiles at $\phi = 0°$ (top) and at $\phi = 90°$ (bottom). The arrows indicate the peak position of scattering profiles.

IV. Discussion

A. Dynamic Phase Diagram. As described in section I, the shear-induced phase separation depends on the relation between the shear rate $\dot{\gamma}$ and the longest relaxation time τ_m of the system. In case of a continuous shear flow, the phase separation occurs only when $\dot{\gamma}$ is larger than τ_m^{-1}. It is natural to consider that the phase separation should also occur under oscillatory shear flow when this condition is satisfied. Because $\dot{\gamma}$ oscillates

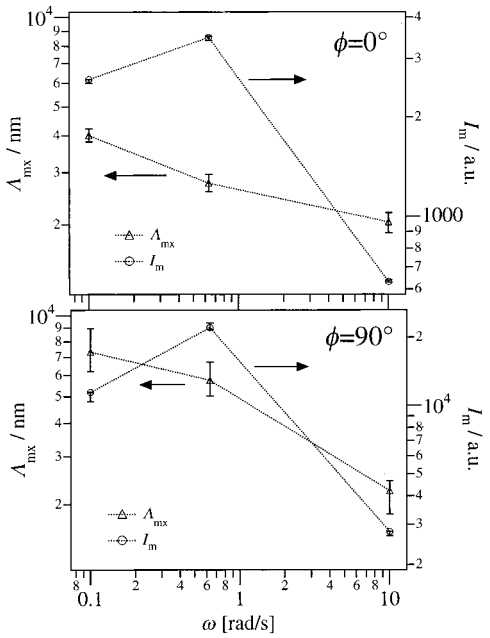

Figure 11. Frequency dependence of Λ_{mx} and I_m evaluated from Figure 10.

with ϕ in the case of an oscillatory shear flow, we use the maximum shear rate $\dot{\gamma}_{max} = \gamma_0\omega$ as a characteristic shear rate. Thus, we compare two values ($\dot{\gamma}_{max}$ and τ_m^{-1}) in order to get the condition necessary for phase separation.

Another time scale plays an important role in the shear-induced phase separation. This is the rate required for the solvent squeezing τ_s^{-1}, which is equivalent to the growth rate of concentration fluctuations induced by shear flow. As shown in Figure 1, the concentration fluctuations or phase separation are built up under shear by squeezing solvent from the more entangled regions in a single phase. τ_s^{-1} might depend on both q and $\dot{\gamma}$, but here we regard, for simplicity, this as a value unique to the system. It is useful to compare τ_s^{-1} and angular frequency ω because the period given for growth of concentration fluctuations under oscillatory shear flow is a quarter of a shearing cycle (from 0° to 90° or from 180° to 270°), as indicated in section III.B.

We shall now qualitatively explain the dynamic phase diagram shown in Figure 5 by considering the relation among the following four quantities, i.e., $\dot{\gamma}_{max}$, τ_m^{-1}, τ_s^{-1}, and ω.

First, we try to compare $\dot{\gamma}_{max}$ and τ_m^{-1}. Suppose that oscillatory shear flow which has maximum shear rate $\dot{\gamma}_{max} = \gamma_0\omega$ is imposed on the system. The stress or the elastic free energy stored by deformation of the entangled polymer solution is relaxed by disentanglement when $\dot{\gamma}_{max}$ is smaller than τ_m^{-1}. When $\dot{\gamma}_{max}$ is larger than τ_m^{-1}, as discussed in section I, the elastic free energy is released not by the disentanglement but by the solvent squeezing, and shear-induced structures are developed from the single-phase solution. As a result, $\dot{\gamma}_{max} = \gamma_0\omega > \tau_m^{-1}$ becomes crucial for phase separation induced by oscillatory shear flow. If γ_0 is relatively small, ω is necessary to be sufficient to induce phase separation, and if γ_0 is relatively large, phase separation could be induced even at a low ω. Thus, the $\gamma_0\omega = \tau_m^{-1}$ line in the γ_0−log ω space becomes the left part of a quasi-parabolic line in Figure 5.

Second, let us compare ω and τ_s^{-1} to explain the right part of the quasi-parabolic line in Figure 5. Consider the oscillatory shear flow with angular frequency ω is imposed on the system. In this case, the higher the value ω, the shorter the time available for formation of the shear-induced structures. If ω is lower than τ_s^{-1}, a phase separation occurs because there is enough time for the solvent squeezing within a shearing cycle. However, if ω is higher than τ_s^{-1}, concentration fluctuations should not grow in a shearing cycle, and the entangled polymer network is only deformed periodically without the solvent squeeze. Consequently, the shear-induced phase separation should not occur. Therefore, $\omega < \tau_s^{-1}$ is one of the indispensable conditions for phase separation, and the $\omega = \tau_s^{-1}$ line in the γ_0−log ω space becomes the right part of a quasi-parabolic line in Figure 5.

Note that there is a possibility that shear-induced structures might be developed at an even higher ω at the spatial scale corresponding to a higher q region out of our experimental window ($q \geq 3.43 \times 10^{-3}$ nm^{-1}). This is because at the higher q we are concerned with structures at a shorter length scale, for which the time for the solvent squeezing is shorter. Hence, the shear-induced structures may be formed at the higher ω. In fact, our recent experiments with small-angle neutron scattering (SANS) revealed that shear-induced butterfly patterns are observed under an oscillatory shear flow with a large strain amplitude even at the q scale of SANS.[21] However, at an extremely high ω, structures with the spatial scale smaller than the mesh size of entangled polymer chain would respond to the oscillatory shear deformation. Under this condition the solvent squeezing would never occur. Therefore, it is reasonable to suppose that shear-induced phase separation does not occur at ω's higher than the critical value.

It follows that the conditions $\gamma_0\omega > \tau_m^{-1}$ and $\omega < \tau_s^{-1}$ are indispensable to induce phase separation under the oscillatory shear flow, and we can obtain a quasi-parabolic line on the dynamic phase diagram by drawing the lines given by $\gamma_0\omega = \tau_m^{-1}$ and $\omega = \tau_s^{-1}$. Moreover, these two conditions strongly depend on the rheological and thermodynamic properties of a system, and if these properties of a system change, the quasi-parabolic line on the dynamic phase diagram will change its shape and position.

B. Angular Frequency Dependence of Dynamic Properties of Shear-Induced Structures. In a period of the shearing cycle, we found that the shear-induced structures developed and decayed synchronously with the strain phase, independently of ω for ω satisfying $\omega_{c,L} < \omega < \omega_{c,H}$, where $\omega_{c,L}$ and $\omega_{c,H}$ are the lower and upper bounds for the shear-induced structures, respectively. Furthermore, we found out that the dynamics of the shear-induced structures depends on ω. In the case of $\omega = 0.1$ rad/s, the scattering intensity increased and decreased with ϕ at all q window covered in this experiment. However, in the case of $\omega = 10$ rad/s, the q region could be divided into that where $I(\mathbf{q})$ depends on ϕ, where the scattering intensity oscillates with ϕ, and that where $I(\mathbf{q})$ is almost independent of ϕ. To consider this difference between 0.1 and 10 rad/s, we show the ratio of the intensity at the strain phase $\phi = 90°$ to that at $\phi = 0°$ as a function of q defined as follows:

$$r(q_x; \omega) = I(q_x, \phi = 90°; \omega)/I(q_x, \phi = 0°; \omega) \quad (5)$$

The ratio $r(q_x;\omega)$ at $\omega = 0.6309$ rad/s, which is the value ω in between 0.1 and 10 rad/s, is included in Figure 12, because the ω dependence of $r(q_x;\omega)$ becomes clearer by including these data. The value q_x at the peak position

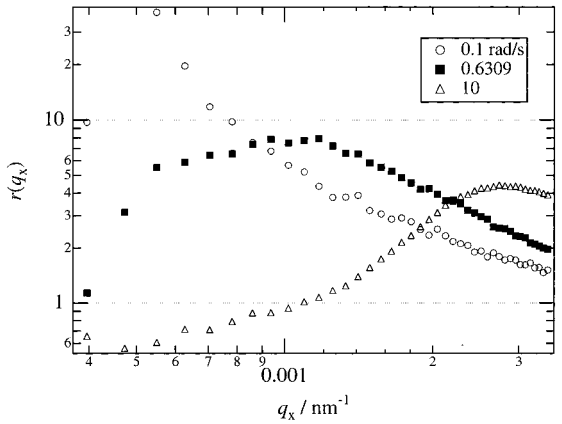

Figure 12. Intensity ratio $r(q_x;\omega)$ along the flow direction at $\omega = 0.1$, 0.6309, and 10 rad/s.

of the scattering intensity, defined as q_x*, roughly corresponds to the q_x where the scattering intensity exhibited the largest change in a shearing cycle. With $r(q_x;\omega) = 1$ the scattering intensity does not change in a shearing cycle. The ratios $r(q_x;\omega)$ at $\omega = 0.1$ and 0.6309 rad/s are beyond the line of 1. However, at $\omega = 10$ rad/s it is nearly equal to 1 below $q_x \cong 0.001$ nm^{-1}, although the downward deviation from 1 exists, which was caused by the artificial scattering appeared in the low-q region.[22] It becomes greater than 1 at q_x greater than 0.0012 nm^{-1} and maximum at $q_x \cong 0.003$ nm^{-1}.

As ω increased, q_x* moved to a higher q_x and $r(q_x$*$;\omega)$ decreased, although q_x* at 0.1 rad/s cannot be found clearly. We may speculate that q_x* exists in a small q region outside the q window of our measurements. This indicates that the characteristic size of structures developed and decayed in a shearing cycle becomes small with increasing ω. We believe that this is because the time available for the structural response in a shearing cycle becomes shorter with an increase of ω. Especially in the case of 10 rad/s, the large length scale structures, the response of which is reflected in $r(q_x;\omega)$ in the low-q_x region, have a relatively long response time (relaxation time) and cannot be developed and relaxed with the applied shear. On the other hand, small length scale structures, the response of which is reflected in $r(q_x;\omega)$ in the high-q_x region, has a short response time or relaxation time and can be developed and relaxed with the shear.

C. Angular Frequency Dependence of Shear-Induced Structures. Here we shall concentrate on the properties of the shear-induced structures at the representative ϕ in terms of size Λ_{mx} and magnitude of the concentration fluctuations. The ω dependence of Λ_{mx} at $\phi = 0°$ and 90° in Figure 11 indicates that the characteristic size of shear-induced structures at a representative ϕ decreases as ω increases. This result could be explained by a similar discussion presented in sections IV.A and IV.B. In the case of the oscillatory shear flow, the spatial scale of the structures depends on ω; the larger the value ω, the shorter the time available for the shear-induced structure formation, and hence the length scale of the shear-induced structures at a representative ϕ at dynamic steady state becomes smaller.

On the other hand, I_m took a maximum at $\omega = 0.6309$ rad/s, implying that the magnitude of the concentration fluctuations, i.e., the scattering contrast between two phases, reaches a maximum at this ω.

To confirm this interpretation, let us attempt to estimate the magnitude of the concentration fluctuations from the scattering patterns. The mean square of the magnitude of the concentration fluctuations $\langle\eta^2\rangle$ is estimated from an invariant Q:

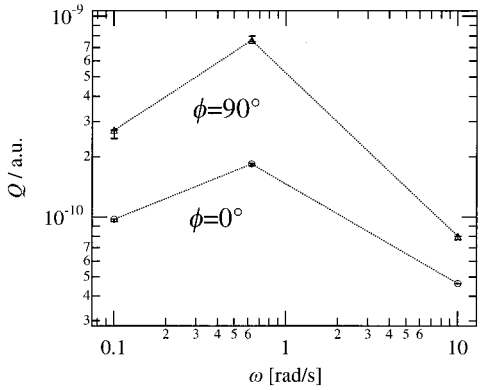

Figure 13. Frequency dependence of invariant Q at $\phi = 0°$ and 90°.

$$\langle\eta^2\rangle \sim Q \equiv \int I(\mathbf{q})\, d\mathbf{q} \tag{6}$$

where the integration is carried out over the whole **q** space. For an isotropic system, Q is estimated from the $|\mathbf{q}|$ dependence of $I(q)$, i.e., one-dimensional scattering intensity distribution. For an anisotropic system like a sheared system, however, a three-dimensional distribution of $I(\mathbf{q})$ over the whole **q** space is needed for the estimation of Q. In our experiments, we measured only a two-dimensional distribution of $I(\mathbf{q})$ in the q_x-q_z plane because of the limitation of the apparatus. To calculate Q for the butterfly patterns obtained in our experiments, we assume that the system has the cylindrically symmetric structure around the x axis.[23] On this assumption, the scattering intensity distribution also exhibits the cylindrical symmetry around the q_x axis. Then we obtain from eq 6

$$\langle\eta^2\rangle \sim Q \cong \int_0^{\pi}\int_{q_1}^{q_2} I(q) q^2 \sin\varphi\, dq\, d\varphi \tag{7}$$

where φ is the azimuthal angle around the q_x axis, and q_1 (=3.96 × 10^{-4} nm^{-1}) and q_2 (=3.43 × 10^{-3} nm^{-1}) are the lower and upper limits of q, respectively, between which the intensity was measured experimentally along the q_x direction. Thus, we calculated Q and plotted it as a function of ω at $\phi = 0°$ and 90° as shown in Figure 13. It is clear that the magnitude of the concentration fluctuations takes a maximum at a proper ω.

To give an account of the behavior of Q against ω, we shall propose the following two opposite quantities: one is the driving force of phase separation induced by the oscillatory shear flow, which promotes the growth in size and magnitude of the concentration fluctuations for the shear-induced structures, and the other is the time available for growth of concentration fluctuations driven by the oscillatory shear flow, which restricts their size and magnitude. The driving force of phase separation depends on $\gamma_0\omega$, i.e., the maximum shear rate given to the system by the oscillatory shear flow (eq 2). The time available for growth of the concentration fluctuations is equivalent to the time available for squeezing solvent, and this is proportional to a period of the shearing cycle.

When ω is relatively low ($\omega = 0.1$ rad/s), the time available for growth of concentration fluctuations is sufficiently long. However, the driving force of phase separation is small. As a result, the magnitude of the

concentration fluctuations cannot become large. On the contrary, when ω is relatively high ($\omega = 10$ rad/s), the time available for growth of the concentration fluctuations is short, though the driving force of phase separation is large; therefore, the magnitude of the concentration fluctuations is still small. Only when ω has an appropriate value between them ($\omega = 0.6309$ rad/s) are both the driving force of phase separation and the period for growth of the concentration fluctuations sufficient, so that the magnitude of the concentration fluctuations can become large.

It should be also noted that the change in $\langle\eta^2\rangle$ in a shearing cycle can be estimated from Figure 13. Since we have pointed out that the shear-induced structures in a shearing cycle changed in harmony with ϕ for all angular frequencies covered in this work, the change in $\langle\eta^2\rangle$ in a shearing cycle is given by the difference between Q at 90° and Q at 0°. It is quite sure that the ω dependence of this value has the same trend with that of Q at 0° and 90°.

D. Comparison with the Results of the Continuous Shear Flow. There have been many reports of continuous-shear-induced phase separation in semidilute polymer solutions near the Θ condition.[1−5,11−19,24−29] Our experiment and discussion show that the oscillatory shear also could induce phase separation. When we compare the previous reports with ours, some distinct similarities and differences are found.

First, we point out the similarity between the time evolution of the shear-induced structures after imposing continuous shear flow and dynamic behavior of the shear-induced structures in a shearing cycle under oscillatory shear flow. Kume et al.[4] reported the transient behavior of the scattering and rheological properties of the same system after onset of imposing a continuous shear flow. After imposing the continuous shear flow, the butterfly type scattering pattern appears, and the scattering peak position moved to a smaller q and the scattering intensity at the peak position increased with increasing time, and finally the system reached the steady state. This process is very similar to that in spinodal decomposition in a thermodynamically unstable solution without shear. Although not reported here, a similar tendency was observed in ϕ-dependent structural change in a shearing cycle. The results shown in Figures 7 and 9 through the process from $\phi = 0°$ to 90° bear a qualitative resemblance to that of Kume's report. It is reasonable to suppose that the transient behavior after onset of the continuous shear flow is reproduced in the structural change or the change in $I(q_x)$ as ϕ increased from 0° to 90° at a dynamic steady state, while these structures are decayed as ϕ increased from 90° to 180°. At least one may recognize a similarity in the two systems in terms of deformation of entangled networks and the solvent squeeze.

Second, the following difference in the static properties of the shear-induced structures should be noticed. In the case of continuous shear flow, almost all the experimental results indicated that the scattering profile along the flow direction at the steady state is very broad without the scattering peak over the q window covered, and even if the scattering peak existed, it was very broad. On the other hand, as indicated in Figures 7 and 9, the scattering profiles under the oscillatory shear flow have a clear scattering peak. This indicates that the size distribution of structures induced by oscillatory shear flow is narrower than those induced by the continuous shear flow. The continuous shear flow affects or enhances all the Fourier modes of concentration fluctuations having the relaxation rate larger than shear rate. Oscillatory shear flow enhances only the concentration fluctuations having the relaxation rate nearly equal to the angular frequency of a given oscillatory shear. As a result, the structures having a relatively narrow size distribution are produced.

Finally, it should be pointed out that the streaklike scattering pattern,[11] which appears in the direction perpendicular to flow at a very high shear rate when continuous shear flow is imposed, could not be observed under the oscillatory shear flow. This streaklike pattern originates in the stringlike structures oriented parallel to flow. To obtain the string phase under oscillatory shear flow, a large strain amplitude would be necessary to get a high shear rate.

V. Conclusions

We performed the in-situ, time-resolved small-angle light scattering experiment to investigate the phase separation of a semidilute solution comprised of ultrahigh molecular weight polystyrene and dioctyl phthalate under oscillatory shear flow. First we showed that oscillatory shear flow also induced phase separation similarly to continuous shear flow, and its occurrence strongly depended on γ_0 and ω. The γ_0−log ω plane could be divided into one-phase and two-phase regions, and hence a sort of dynamic phase diagram was obtained.

The shear-induced structures in a shearing cycle changed in harmony with strain phase ϕ independent of ω when ω satisfies the criterion of the shear-induced phase separation: The structures developed from $\phi =$ 0° to 90° and decayed from 90° to 180°. The characteristic size of the structures developed and decayed in a shearing cycle becomes smaller with an increase of ω, because the time available for the shear-induced structure formation becomes shorter with ω. On the other hand, the mean square of the concentration fluctuations $\langle\eta^2\rangle$ took a maximum at a certain ω because of ω-dependent competition between the driving force of phase separation and the time available for the solvent squeeze.

References and Notes

(1) Hashimoto, T.; Takebe, T.; Fujioka, K. In *4th Nishinomiya-Yukawa Symposium on Theoretical Physics; Dynamics and Patterns in Complex Fluids*; Onuki, A., Kawasaki, K., Eds.; Springer: Heidelberg, 1990; p 86 and references therein.
(2) Hashimoto, T.; Fujioka, K. *J. Phys. Soc. Jpn.* **1991**, *60*, 356.
(3) Hashimoto, T.; Kume, T. *J. Phys. Soc. Jpn.* **1992**, *61*, 1839.
(4) Kume, T.; Hattori, T.; Hashimoto, T. *Macromolecules* **1997**, *30*, 427.
(5) Moses, E.; Kume, T.; Hashimoto, T. *Phys. Rev. Lett.* **1994**, *72*, 2037.
(6) Helfand, E.; Fredrickson, G. H. *Phys. Rev. Lett.* **1989**, *62*, 2468.
(7) Onuki, A. *Phys. Rev. Lett.* **1989**, *62*, 2472.
(8) Onuki, A. *J. Phys. Soc. Jpn.* **1990**, *59*, 3427.
(9) Onuki, A.; Yamamoto, R.; Taniguchi, T. *J. Phys. II* **1997**, *7*, 295.
(10) Doi, M.; Onuki, A. *J. Phys. II* **1992**, *2*, 1631.
(11) Kume, T.; Hashimoto, T. In *Flow-Induced Structure in Polymers*; Nakatani, A. I., Dadmun, M. D., Eds.; American Chemical Society: Washington, DC, 1995; p 35.
(12) Kume, T.; Hashimoto, T.; Takahashi, T.; Fuller, G. G. *Macromolecules* **1997**, *30*, 7232.
(13) Dixon, P. K.; Pine, D. J.; Wu, X.-L. *Phys. Rev. Lett.* **1992**, *68*, 2239.

(14) Murase, H.; Kume, T.; Hashimoto, T.; Ohta, Y.; Mizukami, T. *Macromolecules* **1995**, *28*, 7724.
(15) Wirtz, D. *Phys. Rev. E* **1994**, *50*, 1755.
(16) Wirtz, D. *Macromolecules* **1994**, *27*, 5639.
(17) Wu, X.-L.; Pine, D. J.; Dixon, P. K. *Phys. Rev. Lett.* **1991**, *66*, 2408.
(18) Yanase, H.; Moldenaers, P.; Mewis, J.; Abetz, V.; van Egmond, J.; Fuller, G. G. *Rheol. Acta* **1991**, *30*.
(19) Moldenaers, P.; Yanase, H.; Mewis, J.; Fuller, G. G.; Lee, C.-S.; Magda, J. J. *Rheol. Acta* **1993**, *32*, 1.
(20) Matsuzaka, K.; Hashimoto, T. *Rev. Sci. Instrum.* **1999**, *70*, 2387.
(21) Saito, S.; Matsuzaka, K.; Koizumi, S.; Suehiro, S.; Hashimoto, T., manuscript in preparation.
(22) This artificial scattering arose from the tiny bubbles which could not be removed when the solution was put into the shear cell.
(23) Light scattering experiments show that the PS/DOP subjected to continuous shear flow at high shear rates exhibits the butterfly pattern in the q_x-q_y plane similar to that obtained in the q_x-q_z plane.[13,15−17] This indicates that the assumption proposed here is not far from the truth.
(24) Boue, F.; Lindner, P. *Europhys. Lett.* **1994**, *25*, 421.
(25) Fuller, G.; van Egmond, J.; Wirtz, D.; Peuvrel-Disdier, E.; Wheeler, E.; Takahashi, T. In *Flow-Induced Structure in Polymers*; Nakatani, A. I., Dadmun, M. D., Eds.; American Chemical Society: Washington, DC, 1995; p 22.
(26) Larson, R. G. *Rheol. Acta* **1992**, *31*, 497.
(27) Nakatani, A. I.; Douglas, J. F.; Ban, T.-B.; Han, C. C. *J. Chem. Phys.* **1994**, *100*, 3224.
(28) Rangel-Nafaile, C.; Metzner, A. B.; Wissbrun, K. F. *Macromolecules* **1984**, *17*, 1187.
(29) van Egmond, J. W.; Werner, D. E.; Fuller, G. G. *J. Chem. Phys.* **1992**, *96*, 7742.

MA990031I